Available online at www.sciencedirect.com
ScienceDirect
Journal of Power Sources 165 (2007) 413–419
JOURNAL OF POWER SOURCES
www.elsevier.com/locate/jpowsour

Laser-printed thick-film electrodes for solid-state rechargeable Li-ion microbatteries

Heungsoo Kim *, Raymond C.Y. Auyeung, Alberto Piqué

Materials Science and Technology Division, Naval Research Laboratory, Washington, DC, USA

Received 25 October 2006; received in revised form 28 November 2006; accepted 28 November 2006
Available online 22 January 2007

Abstract

Laser-printed thick-film electrodes ($LiCoO_2$ cathode and carbon anode) are deposited onto metallic current collectors for fabricating Li-ion microbatteries. These microbatteries demonstrate a significantly higher discharge capacity, power and energy densities than those made by sputter-deposited thin-film techniques. This increased performance is attributed to the porous structure of the laser-printed electrodes, which allows improved ionic and electronic transport through the thick electrodes (~100 μm) without a significant increase in internal resistance. These laser-printed electrodes are separated by a laser-cut porous membrane impregnated with a gel polymer electrolyte (GPE) in order to build mm-size scale solid-state rechargeable Li-ion microbatteries ($LiCoO_2$/GPE/carbon). The resulting packaged microbatteries exhibit a power density of ~38 mW cm^{-2} with a discharge capacity of ~102 μAh cm^{-2} at a high discharge rate of 10 mA cm^{-2}. The laser-printed microbatteries also exhibit discharge capacities in excess of 2500 μAh cm^{-2} at a current density of 100 μA cm^{-2}. This is over an order of magnitude higher than that observed for sputter-deposited thin-film microbatteries (~160 μAh cm^{-2}).
Published by Elsevier B.V.

Keywords: Thick-film electrodes; Laser direct-write; Li-ion microbattery; Gel polymer electrolyte

1. Introduction

There is an increasing demand for rechargeable micropower sources for the development of autonomous microelectronic devices such as wireless network microsensors. Thin-film Li and Li-ion microbatteries are being studied as a potential micropower source for developing microelectronic devices due to their high operating voltages, high energy densities and long cycle life [1–3]. These rechargeable thin-film microbatteries are prepared with crystalline cathode films (lithium-transition metal oxides) by sputtering [1–4], pulsed laser deposition (PLD) [5], chemical vapor deposition [6], and sol–gel [7] techniques. However, the thicknesses of the cathode films prepared by these thin-film processing techniques are typically limited to 1–5 μm due to several factors such as adhesion and internal resistance. Dudney and Jang demonstrate that Li–$LiCoO_2$ solid-state thin-film microbatteries with a cathode thickness of 4 μm only deliver ~70% of the maximum capacity, whereas the thinner cathodes (<1 μm) supply as much as ~95% of the maximum capacity [2]. The discharge capacity of the thicker $LiCoO_2$ cathode films decreases more rapidly with increasing discharge current density [2]. This is attributed to the relatively high internal cell resistance of the thicker, denser cathodes, which limits the diffusivity of lithium ions. Because of this thickness limitation, the power and capacity per active electrode area of the thin-film microbatteries are not sufficient to operate many microelectronic devices.

One promising approach to overcome the thickness limitation (i.e., low power and energy density) in thin-film microbatteries is to develop thick-film electrodes using the laser direct-write technique or LDW, which is a laser printing process. LDW allows for the fabrication of highly porous structured thick-film electrodes [8,9] without the need of any lithographic patterning steps. In LDW, a laser pulse is employed to transfer or print 3D pixels or voxels of an ink or paste containing a suspension of the electrode materials onto a substrate in order to form a pattern. Processing can convert the laser-printed patterns into a porous thick-film structure ideally suited for microbattery applications. Laser-printed electrodes could provide much higher capacities per electrode area than the sputter-deposited thin-film electrodes, since their porous structure allows better

* Corresponding author. Tel.: +1 202 404 2094; fax: +1 202 767 1697.
E-mail address: hskim@ccs.nrl.navy.mil (H. Kim).

0378-7753/$ – see front matter. Published by Elsevier B.V.
doi:10.1016/j.jpowsour.2006.11.053

ionic and electronic transport through the thick electrodes (~100 μm) without a significant internal resistance. The LDW technique also can directly embed the electrochemical component into the substrates, reducing the size and weight of the microdevices [10]. Furthermore, this process can be combined with *in situ* laser annealing for processing the layers of active materials without damaging the substrate underneath, which is ideally suited for developing power sources on flexible plastic substrates [9]. This LDW technique has successfully fabricated Li- and Li-ion microbatteries using $LiCoO_2$ cathodes, carbon or Li anodes, and laser-transferable polymer-ionic liquid separator/electrolytes and liquid electrolytes [10–12]. In this study, we demonstrate an order of magnitude higher power and capacities in high discharge current regimes up to 10 mA cm^{-2} for Li-ion microbatteries fabricated with gel polymer electrolytes and much thicker electrodes (36–130 μm).

The current Li-ion battery systems consist of a $LiCoO_2$ cathode, a carbon/graphite anode, and a liquid electrolyte with an alkyl carbonate organic solvent. However, leakage and safety issues (flammability and instability at high temperatures) limit the utility of liquid electrolytes. One way to overcome these difficulties is to use gel polymer electrolytes (GPEs) by incorporating liquid electrolytes (high ionic conductivity) into a polymer matrix (removal of electrolyte leakage problem). Several GPEs have been investigated including poly(ethylene oxide) (PEO) [13], polymethylmethacrylate (PMMA) [14], polyacrylonitrile (PAN) [15], and polyvinylidene fluoride (PVdF) [16–18]. Among these polymers, PVdF and its hexafluoropropylene (HFP) copolymer, PVdF–HFP, are of considerable practical interest due to its wide scale availability and its superior electrochemical properties. Bellcore (now Telcordia Technologies) produces a plastic Li-ion battery using a microporous plasticized PVdF–HFP based polymer electrolyte [19]. In this case, the anode and cathode are laminated onto either side of a gel polymer electrolyte, which serves both as electrolyte and separator. However, the mechanical properties of the 75 μm thick separators used in these cells appeared to be very poor [19]. In this work, in order to avoid any problems due to poor mechanical properties, a PVdF–HFP based gel polymer electrolyte infuses a microporous membrane, which also serves as a separator for Li-ion microbatteries.

In this paper, we detail the high capacity and high discharge rate capability of thick-film Li-ion microbatteries, fabricated using laser-printed thick-film electrodes ($LiCoO_2$ cathode and carbon anode) with GPE soaked membranes. Once printed, the microbatteries are assembled and packaged in a glove box and tested in air. The influence of electrode thickness on the battery performance is then studied. High discharge capacities of >2.5 mAh cm^{-2} are demonstrated. The performance of the thick-film Li-ion microbatteries is also compared with those results reported in the literature for microbatteries prepared by sputter-deposited thin-film electrodes.

2. Experimental

The cathode ink is prepared by mixing 91% $LiCoO_2$ (CO22, Seimi), 4% graphite (KS6, Timcal), 2% carbon black (Super P, Erachem) in a solution of 3% PVdF–HFP (Kynar 2801, Elf Atochem) in dibasic ester (DBE, a blend comprised of 59 wt.% dimethyl gluturate, 21 wt.% dimethyl adipate, and 20 wt.% dimethyl succinate, Du Pont) solvent. The anode ink consists of 91% carbon (MCMB 2528, Osaka Gas), 1% carbon black, and 8% PVdF–HFP in DBE solvent. The cathode and anode electrodes are laser-printed onto 50 μm thick Al and Cu current collectors, respectively. Fig. 1 is a schematic diagram of the laser direct-write setup used for this work. Details of the laser printing process have been described previously [8,20]. Briefly, the ink is uniformly spread onto a borosilicate glass slide using a wire coater (#5, Garner) and then irradiated by a frequency-tripled Nd:YVO_4 laser ($\lambda = 355$ nm) focused to a 50 μm × 50 μm spot. Each laser pulse results in the forward transfer of a voxel of ink across a 100 μm gap separating the receiving substrate from the ink-coated ribbon. The laser fluence is maintained at ~50–100 mJ cm^{-2}, while the number of transfer passes is varied to control the transferred film thickness. The active area of the electrode is 0.49 cm^2. The laser-printed electrodes are dried in a vacuum oven at 120 °C for 24 h in order to remove the DBE solvent and any absorbed water. The dried electrodes are then transferred to a glove box (Ar, O_2, and H_2O < 1 ppm) and stored for 24 h prior to assembly, allowing the absorbed oxygen and moisture in the electrodes to equilibrate with the levels of the glove box.

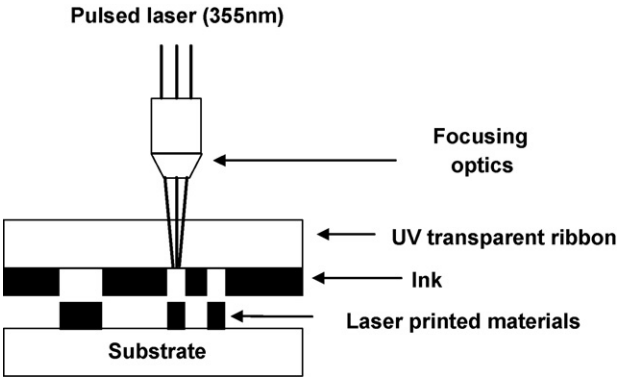

Fig. 1. A schematic diagram of an LDW system.

The gel polymer electrolytes (GPEs) are prepared in the glove box by mixing a polymer matrix and a liquid electrolyte. PVdF–HFP is used as the polymer matrix for the GPE. A solution of 1 M $LiPF_6$ (Aldrich) in propylene carbonate (PC)/ethylene carbonate (EC)/dimethyl carbonate (DMC) (1:1:3 by volume, used as received from Aldrich) is used as a liquid electrolyte. PVdF–HFP powder is dissolved into the liquid electrolyte solution by stirring at 60 °C. A polyolefin based microporous membrane (E25MMS SETELA, Tonen Chemical Corp.) is used as a separator. The 25 μm thick membrane is laser-cut into 8 mm × 8 mm pieces, which are then immersed in the GPE solution for 20 min inside the glove box.

The Li-ion microbatteries used for this work are assembled by placing the GPE soaked porous membrane between the $LiCoO_2$ cathode and the MCMB anode. Once assembled, each microbattery is packaged using an airtight seal so that it can be tested outside the glove box. In order to package the

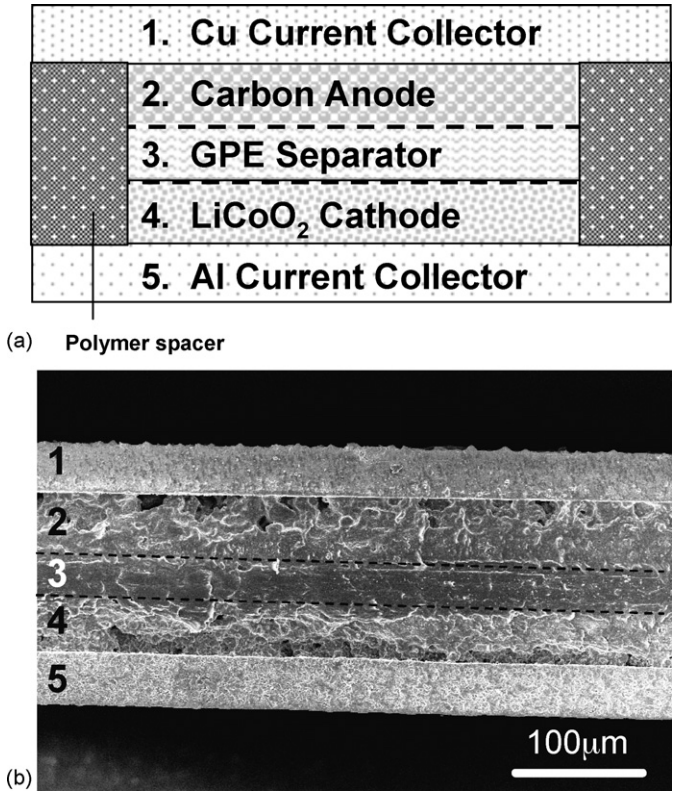

Fig. 2. (a) Cross-sectional schematic diagram (not to scale) of a typical Li-ion microbattery used for this work. (b) Cross-sectional SEM micrograph of a packaged thick-film Li-ion microbattery. The layers visible (from top to bottom) are: (1) Cu current collector, (2) carbon anode, (3) GPE soaked separator, (4) $LiCoO_2$ cathode, and (5) Al current collector. The GPE soaked separator is marked by black dashed lines.

stacked assembly, the current collectors are sealed together with a thermally curable polymer spacer (Surlyn SF-71, Flex-O-Glass) placed along each edge of the active electrode area (7 mm × 7 mm). The sealing is performed by hot pressing the thermally curable polymer at ∼100 °C for 10 s and then followed by immediate cold pressing in order to avoid the crystallization of the sealing polymer, which could result in pinhole leaks in the seal. Fig. 2(a) shows a cross sectional schematic diagram of an assembled Li-ion microbattery. The sealed batteries are then cut out to the desired size (1.3 cm × 1.3 cm) using a laser. Microbatteries are typically cycled between 4.2 and 3 V at constant current densities ranging from 100 μA cm^{-2} to 10 mA cm^{-2} using an Arbin battery tester (BT2000, Arbin Instruments) with MITS Pro 3.0 software. All the microbatteries evaluated for this work are tested in air and at room temperature.

3. Results and discussion

Fig. 2(b) shows an SEM micrograph from the cross section of a typical Li-ion microbattery fabricated for this work. The SEM image reveals each of the layers present in these microbatteries as shown schematically in Fig. 2(a). Higher magnification SEM images from the laser-printed cathode ($LiCoO_2$ + graphite + carbon black) and anode (MCMB 2528 + carbon black) layers are shown in Fig. 3(a) and (b), respectively. The agglomerated $LiCoO_2$ powder grains mixed with the much smaller graphite and carbon black (added to improve electrical conductivity) are clearly seen in Fig. 3(a), while the MCMB 2528 spherical particles (MCMB stands for mesocarbon microbeads) mixed with the smaller carbon black can be observed in Fig. 3(b). Both SEM images also show the highly porous structure of both layers. Fig. 3(c) shows one of the assembled, packaged and laser-cut microbatteries used in this work.

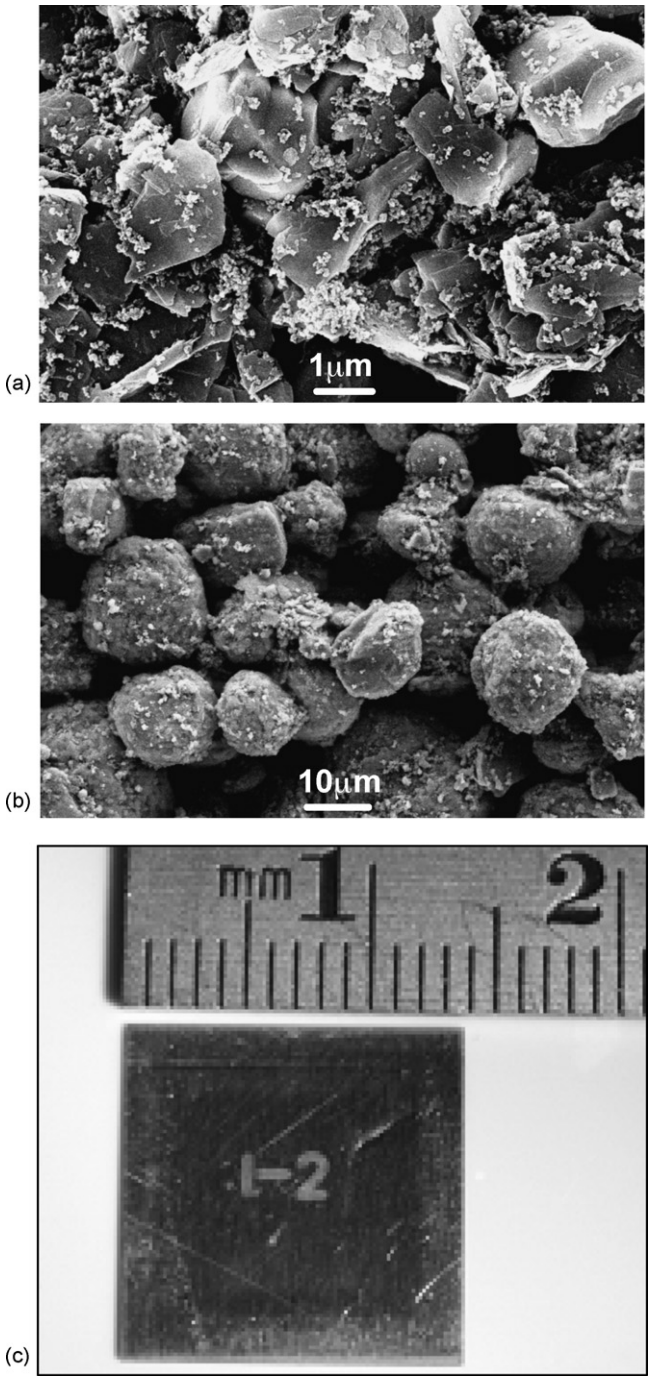

Fig. 3. (a) SEM image of a laser-printed $LiCoO_2$ cathode. (b) SEM image of a laser-printed carbon (MCMB2528) anode. (c) Top view (anode current collector) of a packaged and laser-cut Li-ion microbattery.

Table 1
Microbattery performance as a function of cathode thickness (or LDW passes)

LDW passes	Cathode thickness (μm)	Cathode mass (mg)	Anode thickness (μm)	Anode mass (mg)	Theoretical capacity ratio (cathode/anode)	Discharge capacity at first cycle (μAh cm^{-2})	Specific capacity at first cycle (mAh g^{-1})	Coulombic efficiency at first cycle (%)	Coulombic efficiency at fifth cycle (%)
9×	36	3.30	40	2.54	0.527	867	129	92.1	99.3
12×	52	4.68	58	3.57	0.532	1224	128	90.2	99.1
18×	70	6.39	85	5.37	0.482	1629	125	89.8	99.2
30×	115	10.62	130	8.13	0.530	2586	120	78.8	98.8

The same number of LDW passes is applied to prepare the anode films, which are slightly thicker and lighter than the cathode films. The active electrode area is 0.49 cm^2. Each microbattery is charged/discharged at 100 μA cm^{-2} between 4.2 and 3 V. The microbatteries are packaged in a glove box and tested in air at room temperature.

The printed film thickness is controlled by the number of LDW transfer passes. As shown in Fig. 4(a), the thickness and mass of the $LiCoO_2$ cathode layer are linearly proportional to the number of LDW passes (see also Table 1). After 6 LDW passes (6×) the cathode film thickness and mass are 25 μm and 2.33 mg, respectively, and reach 115 μm and 10.61 mg after 30 LDW passes (30×). The same number of LDW passes is applied to deposit the anode films, which are slightly thicker and lighter than the cathode films. Based on the theoretical capacities of the $LiCoO_2$ cathode ($Li_{0.5}CoO_2$: ~150 mAh g^{-1}) and the MCMB anode (LiC_6: ~370 mAh g^{-1}), all microbatteries made for this work are cathode limited. As shown in Fig. 4(b), the discharge capacities and the cathode mass are proportional to the cathode thickness, indicating that the discharge capacity can be easily controlled by varying the cathode and anode thickness. The viscosity of the ink also affects the film thickness. For high viscosity inks, each LDW pass deposits a thicker film than from a lower viscosity ink. As the viscosity of the inks increases, the laser power required for their transfer increases as well, which can affect the precision of the transfers, as well as alter the film components.

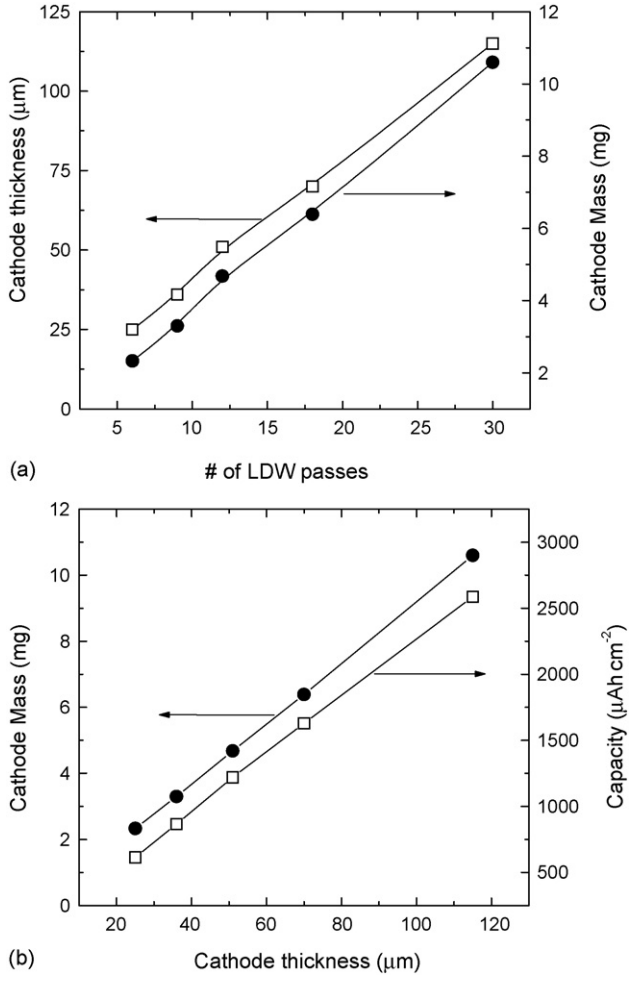

Fig. 4. Plots of (a) cathode thickness and discharge capacity as a function of the number of LDW passes and (b) cathode mass and discharge capacity vs. cathode thickness. The discharge capacity values are obtained at the first cycle of the cells charged and discharged at 100 μA cm^{-2} between 4.2 and 3 V in air. The active electrode area is 0.49 cm^2 for all the cells.

Fig. 5 shows charge/discharge curves for the fifth cycle for packaged Li-ion microbatteries (Al/$LiCoO_2$/GPE-membrane/MCMB/Cu) with cathodes of different thicknesses (36–115 μm). The microbatteries are charged and discharged at a constant current of 100 μA cm^{-2}. The results of the first five charge/discharge cycles of these microbatteries are summarized in Table 1. The achieved discharge capacity per active cathode area is proportional to the cathode thickness. The discharge capacity at the first cycle increases from 867 to 2586 μAh cm^{-2} as the cathode thickness is increased from 36 to 115 μm. The coulombic efficiencies at the first cycle are 92.1, 90.2, 89.8 and 78.8% for 36, 52, 70, and 115 μm thick cathodes, respectively, indicating an irreversible capacity loss of 8–21%. The irreversible capacity losses at the first cycle are attributed to the formation of a solid electrolyte interface (SEI) layer created at the interface between the electrodes and the gel polymer electrolyte due to the decomposition of the electrolyte solvent [21–23]. As shown in Table 1, the first cycle capacity loss depends on the film thickness. Because the GPE permeates into the electrodes, the thicker the electrode, the larger the SEI becomes. Due to the larger SEI layer, the 115 μm thick cathode exhibits a relatively low coulombic efficiency compared to the thinner cathodes. However, by the end of the fifth cycle, the coulombic efficiency of all the microbatteries is greater than 99% and stays almost constant for the rest of the following cycles. The specific discharge capacity based on the mass of cathode material is also compared in Table 1. It can be seen that the discharge capacity per active cathode mass is slightly reduced with increasing electrode thickness. Fig. 5(b) also shows the specific discharge capacity per cathode mass at the fifth cycle.

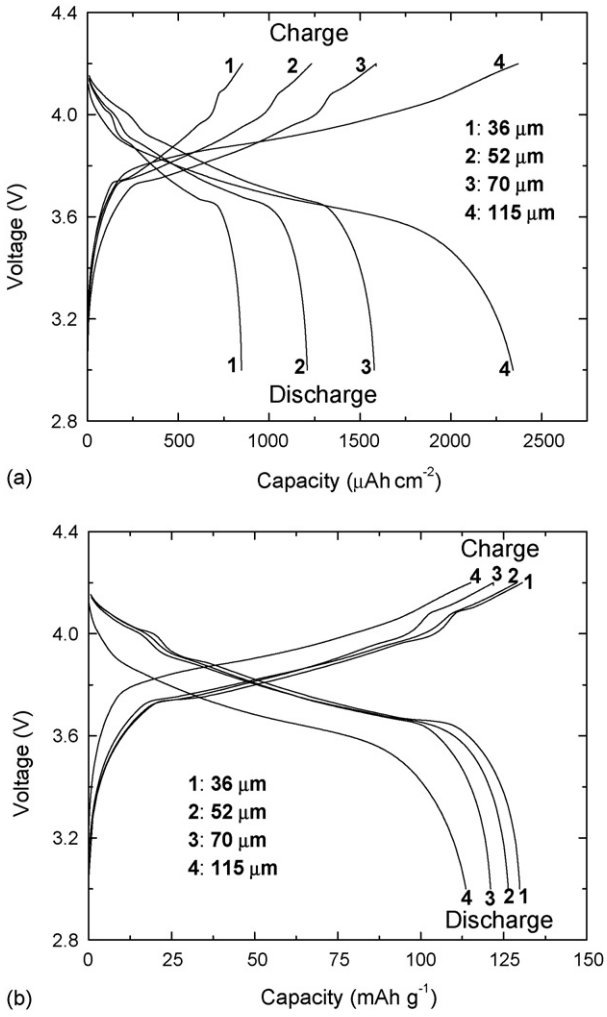

Fig. 5. Charge/discharge curves (fifth cycle) as a function of capacity per (a) active electrode area and (b) cathode mass for packaged Li-ion microbatteries (Al/$LiCoO_2$/GPE/MCMB/Cu) with $LiCoO_2$ cathodes of different thicknesses (36, 52, 70, and 115 μm). Microbatteries are charged at a constant current (100 μA cm^{-2}) between 4.2 and 3 V. The active electrode area is 0.49 cm^2.

Although the specific discharge capacity is lower for the microbattery with the 115 μm thick cathode compared to the battery with the 36 μm thick cathode due to a slightly higher internal resistance, a significantly large discharge capacity per unit area can be achieved for the 115 μm thick cathode.

The discharge rate also affects the capacity of thick-film Li-ion microbatteries. Fig. 6 shows the discharge capacity per active electrode area and cathode mass for thick-film microbatteries with three different cathode thicknesses (21, 45, and 68 μm) as a function of discharge current density (from 100 μA cm^{-2} to 10 mA cm^{-2}). As shown in Fig. 6(a), the slopes of the curves for all the cells are roughly parallel for current densities between 100 and 2000 μA cm^{-2}, indicating that the thickness of the cathode is not a rate limiting factor for Li-ion transport during discharging. This implies that the capacity per unit area can be increased simply by increasing the thickness of the electrodes without any significant internal resistance. However, in the case of the sputter-deposited thin-film Li microbatteries [1], maximum power density is achieved only with the thinnest cathodes (<1 μm) due to their high internal resistance. As seen in Fig. 6(a), the delivered capacities at 100 μA cm^{-2} are 514, 1044, and 1537 μAh cm^{-2} for the 21, 45, and 68 μm thick cathodes, respectively. Assuming that the capacity obtained at 100 μA cm^{-2} represents 100% capacity of the cells, the 21, 45, and 68 μm electrode cells display ~82% (422 μAh cm^{-2}), ~84% (885 μAh cm^{-2}), and ~80% (1224 μAh cm^{-2}) of capacity retention at 1 mA cm^{-2}, respectively. The cell with the 68 μm thick cathode achieves a maximum power density of ~38 mW cm^{-2} (~102 μAh cm^{-2}) at a current density of 10 mA cm^{-2}. As shown in Fig. 6(b), the specific discharge capacities at low current densities (100 μA cm^{-2}) are 130, 125, and 121 mAh g^{-1} for the cells with 21, 45, and 68 μm thick cathodes, respectively, while the specific capacities for all the microbatteries gradually decrease down to ~30 mAh g^{-1} when the discharge rate increases from 100 μA cm^{-2} to 2 mA cm^{-2}. For all ranges of current densities, almost the same fraction of active material in all the cells is accessed for charge/discharge activities. These results confirm that the cathode thickness is not

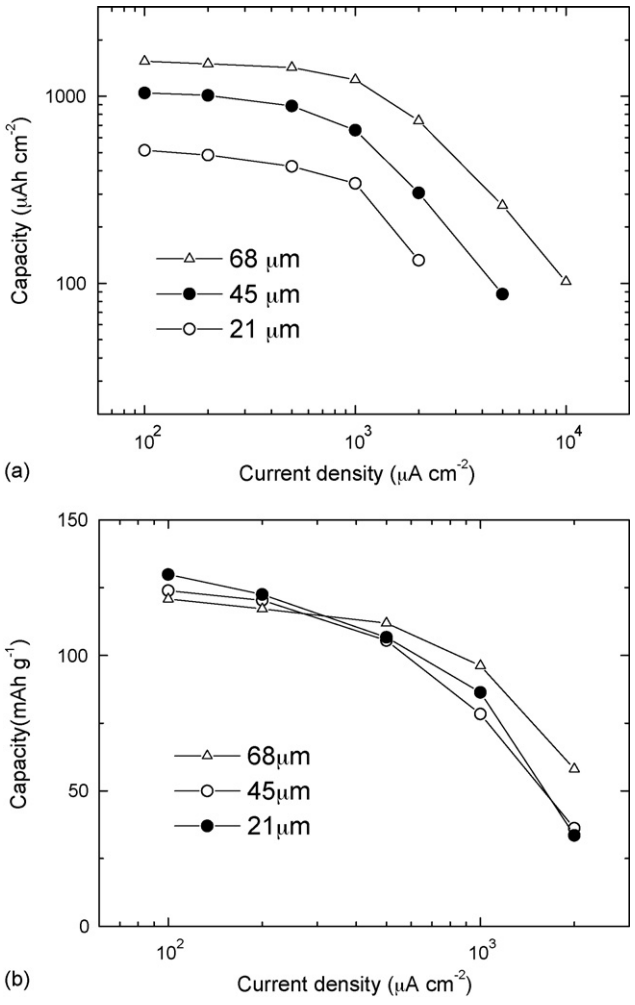

Fig. 6. Discharge capacity per (a) active electrode area and (b) cathode mass for Li-ion microbatteries (Al/$LiCoO_2$/GPE/MCMB/Cu) with $LiCoO_2$ cathodes of different thicknesses (21, 45, and 68 μm). The active electrode area is 0.49 cm^2. Microbatteries are charged at 100 μA cm^{-2} and discharged at various current densities between 4.2 and 3 V in air.

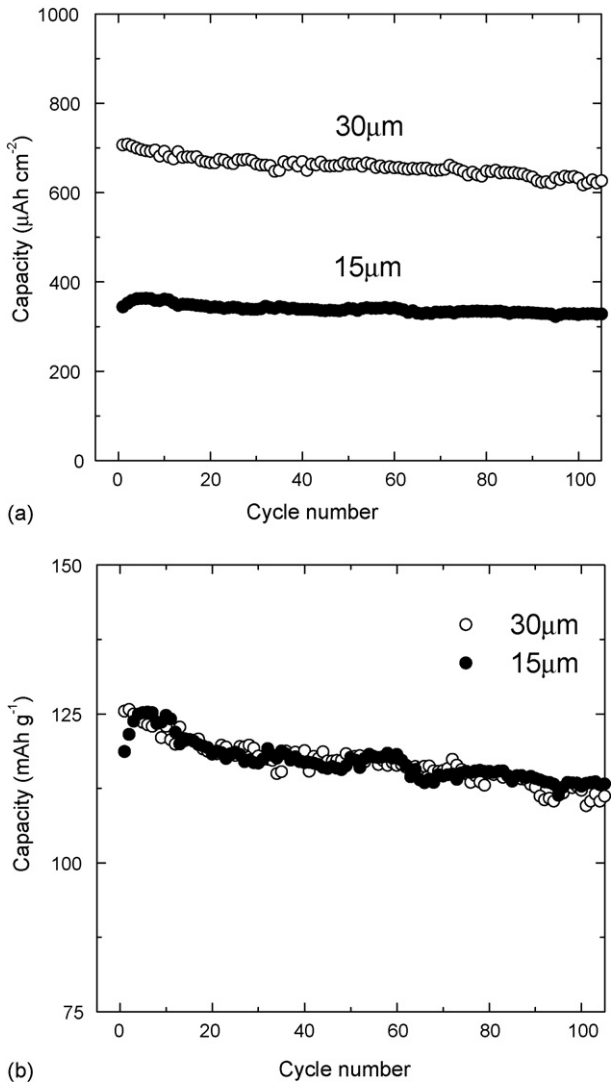

Fig. 7. Cycle performance of two Li-ion microbatteries (Al/$LiCoO_2$/GPE/MCMB/Cu) with different $LiCoO_2$ cathode thicknesses (15 and 30 μm) in terms of (a) discharge capacity per unit area and (b) discharge capacity per cathode mass. The microbatteries are charged/discharged at 100 μA cm^{-2} between 4.2 and 3 V, and each cell had an active electrode area of 0.49 cm^2.

a rate limiting factor for the thick-film microbatteries presented here.

Fig. 7 shows the cycling performance for two Li-ion microbatteries fabricated with different $LiCoO_2$ cathode thicknesses (15 and 30 μm). Each cell is charged and discharged at 100 μA cm^{-2} between 4.2 and 3 V. Both microbatteries show excellent cycling performance over 100 cycles with a slow fade rate of about 0.1% per cycle, which is comparable to those observed for typical Li-ion batteries. This slight fading in discharge capacity with cycling is related to the gradual increase of the SEI layer at the interface between the gel polymer electrolyte and active materials, which in turn raises the internal resistance of the cell. These microbatteries retained about 90% of their initial capacity after 100 cycles. As shown in Fig. 7(b), the discharge capacities based on the mass of the $LiCoO_2$ cathode for both cells are still above 110 mAh g^{-1} after 100 cycles. Based on the volume of active cathode electrodes (area = 0.49 cm^2 area; thickness = 15 and 30 μm), the volumetric energy densities for 15 and 30 μm thick cathodes at the 100th cycle are calculated to be 806 and 779 Wh L^{-1} (or 327 and 632 μAh cm^{-2}), respectively, corresponding to the gravimetric energy density of ~415 Wh kg^{-1} (or 112 mAh g^{-1}) for both Li-ion cells. These results demonstrate the good cycling capability of the laser-printed electrodes operating in ambient atmosphere, made possible by the integrity of the seal used in these thick-film microbatteries.

The discharge capacity per active electrode area of the laser-printed thick-film electrode microbatteries is compared against that of microbatteries fabricated with sputter-deposited thin-film electrodes. For example, Li-microbatteries with sputter-deposited 2.5 μm thick $LiCoO_2$ cathodes (active area = 1 cm^2) display capacities of ~160 μAh cm^{-2} (or ~64 μAh μm^{-1} cm^{-2}) at a current density of 100 μA cm^{-2} [1]. In this work, the Li-ion microbattery with a laser-printed 115 μm thick $LiCoO_2$ (active area = 0.49 cm^2) demonstrated a capacity of ~2586 μAh cm^{-2} (or ~22.5 μAh μm^{-1} cm^{-2}) at the same current density of 100 μA cm^{-2}. Although the volumetric capacity is three times lower than that of the sputter-deposited thin-film cells, the laser-printed thick-film microbatteries can provide order of magnitude higher capacities per unit area. In other words, in order to achieve the same discharge capacity of the laser-printed cell with a 115 μm thick $LiCoO_2$ cathode occupying an area of less than 1/2 cm^2, the sputter-deposited 2.5 μm thick cathode would have to occupy an area 16 times greater or about 8 cm^2. From this comparison, it becomes clear that laser-printed thick-film microbatteries are well suited for applications requiring not only high discharge capacities and high power densities but also limited cell footprints due to size constraints or restrictive form factors as it is the case for wireless network sensor nodes, motes and other autonomous microelectronic systems.

Finally, it is worth noting that the raw materials employed in the preparation of the inks that are used to laser print the cathode ($LiCoO_2$) and anode (MCMB 2528) layers are of the same type as those used for fabricating larger size commercial Li-ion batteries. These materials consist of powders of relatively large particle size, ranging from 1 to 20 μm and are selected due to their superior electrochemical properties. If instead, powders with average sizes under 500 nm and narrower size distributions could be used for making the inks, the resulting laser-printed cathode and anode layers would exhibit greater packing densities, with considerably higher active surfaces. Furthermore, the laser-printed nanoparticles would still form a highly porous agglomerate thus achieving superior ionic and electronic transport properties. Such laser-printed nanostructured microbatteries are expected to achieve volumetric capacities closer to that of the sputter-deposited thin-film microbatteries.

4. Conclusions

Thick-film electrodes ($LiCoO_2$ cathode and carbon anode) are prepared by a laser-printing technique and used to fabri-

cate Li-ion microbatteries with gel polymer electrolyte soaked membranes. These microbatteries are assembled and packaged inside a glove box and then tested in air and at room temperature. Battery performance indicates that the discharge capacities are proportional to the cathode thickness (up to 115 μm thick) without any significant increase in internal resistance. When compared to other types of microbatteries, such as thin-film microbatteries, the laser-printed thick-film microbatteries provided significantly higher discharge capacity ($\sim$2586 μAh cm^{-2}) at a current density of 100 μA cm^{-2}. Such a capacity per unit area is over an order of magnitude higher than that reported for sputter-deposited thin-film microbatteries ($\sim$160 μAh cm^{-2}). A maximum power density of $\sim$38 mW cm^{-2} ($\sim$102 μAh cm^{-2}) is achieved in a microbattery with a 68 μm thick cathode at a current density of 10 mA cm^{-2}. Future experiments would involve laser-printing of nanopowders of the active materials to further improve the volumetric capacities of these cells. Given their higher discharge capacity and high power density per unit area, these laser-printed thick-film microbatteries are ideal for applications where limited space is available for the power source such as in wireless network sensors and other autonomous microelectronic devices.

Acknowledgements

We would like to thank Dr. Tom Sutto for his helpful comments. This work was supported by the Office of Naval Research.

References

[1] J.B. Bates, N.J. Dudney, B. Neudecker, A. Ueda, C.D. Evans, Solid State Ionics 135 (2000) 33–45.
[2] N.J. Dudney, Y.-I. Jang, J. Power Sources 119–121 (2003) 300–304.
[3] B.J. Neudecker, N.J. Dudney, J.B. Bates, J. Electrochem. Soc. 147 (2000) 517–523.
[4] C.-L. Liao, K.-Z. Fung, J. Power Sources 128 (2004) 263–269.
[5] Y. Iriyama, M. Inaba, T. Abe, Z. Ogumi, J. Power Sources 94 (2001) 175–182.
[6] W.-G. Choi, S.-G. Yoon, J. Power Sources 125 (2004) 236–241.
[7] Y.H. Rho, K. Kanamura, M. Fujisaki, J. Hamagami, S. Suda, T. Umegaki, Solid State Ionics 151 (2002) 151–157.
[8] H. Kim, G.P. Kushto, C.B. Arnold, Z.H. Kafafi, A. Piqué, Appl. Phys. Lett. 85 (2004) 464–466.
[9] H. Kim, R.C.Y. Auyeung, M. Ollinger, G.P. Kushto, Z.H. Kafafi, A. Piqué, Appl. Phys. A 83 (2006) 73–76.
[10] T.E. Sutto, M. Ollinger, H. Kim, C.B. Arnold, A. Piqué, Electrochem. Solid State Lett. 9 (2005) A69–A71.
[11] M. Ollinger, H. Kim, T.E. Sutto, A. Piqué, Appl. Surf. Sci. 252 (2006) 8212–8216.
[12] R. Wartena, A.E. Curtright, C.B. Arnold, A. Piqué, K.E. Swider-Lyons, J. Power Sources 126 (2004) 193–202.
[13] J.-H. Shin, W.A. Henderson, S. Scaccia, P.P. Prosini, S. Passerini, J. Power Sources 156 (2006) 560–566.
[14] H.S. Kim, K.S. Kum, W.I. Cho, B.W. Cho, H.W. Rhee, J. Power Sources 124 (2003) 221–224.
[15] H. Akashi, K. Tanaka, K. Sekai, J. Power Sources 104 (2002) 241–247.
[16] P. Arora, Z. Zhang, Chem. Rev. 104 (2004) 4419–4462.
[17] J.Y. Song, Y.Y. Wang, C.C. Wan, J. Power Sources 77 (1999) 183–197.
[18] J.Y. Song, C.L. Chen, Y.Y. Wang, C.C. Wan, J. Electrochem. Soc. 149 (2002) A1230–A1236.
[19] A.D. Pasquier, P.C. Waren, D. Culver, A.S. Gozdz, G. Amatucci, J.M. Tarascon, Proc. Electrochem. Soc. 99 (1999) 360.
[20] A. Piqué, C.B. Arnold, H. Kim, M. Ollinger, T.E. Sutto, Appl. Phys. A 79 (2004) 783–786.
[21] S.S. Zhang, K. Xu, T.R. Jow, Electrochem. Commun. 5 (2003) 979–982.
[22] S. Flandrois, B. Simon, Carbon 137 (1999) 165–180.
[23] M.C. Smart, B.V. Ratnakumar, J.F. Whitacre, L.D. Whitcanack, K.B. Chin, M.D. Rodriguez, D. Zhao, S.G. Greenbaum, S. Surampudi, J. Electrochem. Soc. 152 (2005) A1096–A1104.